Journal Pre-proofs

Self-Assembled Reduced Graphene Oxide Nanoflakes Assisted by Post-Sonication Boosted Electrical Performance in Gold Interdigitated Microelectrodes

S. Taniselass, M.K. Md Arshad, Subash C.B. Gopinath, Muhammad M Ramli

PII: S0021-9797(20)30672-X
DOI: https://doi.org/10.1016/j.jcis.2020.05.070
Reference: YJCIS 26441

To appear in: *Journal of Colloid and Interface Science*

Received Date: 1 January 2020
Revised Date: 16 May 2020
Accepted Date: 18 May 2020

Please cite this article as: S. Taniselass, M.K. Md Arshad, S.C.B. Gopinath, M.M. Ramli, Self-Assembled Reduced Graphene Oxide Nanoflakes Assisted by Post-Sonication Boosted Electrical Performance in Gold Interdigitated Microelectrodes, *Journal of Colloid and Interface Science* (2020), doi: https://doi.org/10.1016/j.jcis.2020.05.070

Self-Assembled Reduced Graphene Oxide Nanoflakes Assisted by Post-Sonication Boosted Electrical Performance in Gold Interdigitated Microelectrodes

S. Taniselass[a,b], M.K. Md Arshad[a,b*], Subash C.B. Gopinath[b,c] , Muhammad M Ramli[a]

[a] School of Microelectronic Engineering, Universiti Malaysia Perlis, Pauh Putra Campus, 02600 Arau, Perlis, Malaysia.

[b] Institute of Nano Electronic Engineering, Universiti Malaysia Perlis, 01000 Kangar, Perlis, Malaysia.

[c] School of Bioprocess Engineering, Universiti Malaysia Perlis, 02600 Arau, Perlis, Malaysia.

Corresponding Author:

* Assoc. Prof. Ir. Dr. Mohd Khairuddin Md Arshad

Tel: +604-9798581; Fax: +604-9798578

Email: mohd.khairuddin@unimap.edu.my

Abstract

Reduced graphene oxide (rGO) is widely utilised to develop various types of biosensors; however, producing self-assembled rGO nanoflake networks through single-droplet drop-casting remains inconsistent. In the present work, we systematically used three different methods to prepare rGO suspensions in order to produce large scale self-assembled rGO nanoflake networks through single-droplet drop-casting. The rGO suspensions were prepared using only deionised water with no added any chemicals/organic solvents, which we considered to be a low-cost method. Subsequently, the most effective preparation method was used to deposit rGO nanoflakes onto commercial gold interdigitated microelectrodes (Au-IDE) to examine their electrical performance. Assessment of the yields, developed methods, surface morphologies, spectroscopy and structural analyses of the as-prepared rGO nanoflakes were conducted. The results revealed that method-3 (involving sonication, centrifugation and post-sonication) produced large self-assembled rGO nanoflake networks with strong adhesion to glass substrates. Furthermore, the as-prepared rGO/Au-IDE modified sensors showed excellent electron mobility where the electrical conductivity was enhanced approximately ~1000 fold compared to the bare devices. The present work provided new insights for depositing large self-assembled interconnected rGO nanoflake networks through single-droplet drop-casting which will be beneficial for biosensor development and other downstream applications.

Keywords: rGO nanoflakes, drop-casting, interdigitated electrodes, post-sonication, impedance

1. Introduction

Two-dimensional (2D) nanomaterial is usually referred to as graphene, because of its uniqueness and far-fetched electrical, mechanical, thermal and optical properties [1]. Graphene is a flat mono-layer of atomic thickness in which carbon atoms are tightly arranged in a honeycomb lattice structure [2]. Graphene-based materials (graphene oxide (GO) and reduced graphene oxide (rGO)) have distinct characteristic values within their properties that make them very attractive as functional nanomaterials for a diverse range of applications [3,4,5]. Among the applications, the most common to date are biosensors, energy storage devices (batteries and supercapacitors), and electronic devices (transistors), used for microwave absorption and as nanocomposite materials for various purposes [6,7,8]. Recently, Shetti et al. developed a novel biosensor, based on graphene oxide and nanoclay, as a nanocomposite for the recognition of the Theophylline drug which is used to treat respiratory-related ailments [9]. However, final-products based on graphene-based materials for consumer-markets, either as biosensors or energy storage devices, are still very rare. This is due to the production of graphene nanosheets suffering from low yield in terms of quantity and quality [10]. Currently, very common methods of producing graphene nanosheets are via micromechanical cleavage, chemical vapor deposition, the unzipping of carbon nanotubes and epitaxial growth [11,12]. However, these methods are unattractive for mass production due to time consuming, tedious procedures that, require high-end equipment, are expensive and produce low yields [13]. These methods are generally used to produce graphene nanosheets for proof-of-concept of their properties, rather than for large-scale production. Nevertheless, chemical routes have paved the way for the more effective scalable production of synthesised graphene-based materials compared to the other aforementioned methods. Recently, a green approach for sustainable environment, which synthesised graphene-based materials, was considered for eliminating the use of hazardous chemicals such as hydrazine [14]. Despite the chemical route being promising for scalable production, the transfer of desirable sizes of graphene nanosheets and its homogenous deposition onto devices/substrates are crucial but challenging tasks. There is a great need for research concerning solutions for the homogenous deposition of graphene-based nanomaterials, particularly in the micro- or nano-regions or within devices.

To date, the deposition methods for graphene-based materials have been based on spray coating [15], spin coating [16], drop-casting [17], dip-coating [18] and electrodeposition [19] which involve deposition onto various electrodes/substrates for numerous applications. Of these methods, the drop-casting technique has been widely used in electrochemical

sensor/biosensor development, because it offers many advantages, such as facility and the elimination of the need for expensive apparatus, making it a cost-effective technique [20,21]. The drop-casting technique enables the deposition of graphene-based materials in very small volumes usually in microliters on microelectrodes' surfaces; for examples, Ozma et al. demonstrated that the drop-casting technique could be successfully implemented to develop a biosensor, using zinc oxide and reduced graphene with Prussian blue for the sensitive detection of Rutin [22]. Meanwhile, Manasa et al. developed an electrochemical sensor, based on a nanocomposite of zinc oxide, reduced graphene oxide and cetyltrimethylammonium bromide which was deposited through the drop-casting technique. They reported that the developed sensor displayed ultrasensitive detection of Bisphenol , with a detection limit of 0.06 μM [23]. Nevertheless, the technique still suffered on attaining a homogenous coating, due to the random dispersion of graphene-based materials in liquid media.

This article reports a new and facile method of homogenously depositing large self-assembled rGO nanoflake networks onto glass substrates through single-droplet drop-casting. The self-assembled rGO nanoflake networks were achieved through existing nanomaterial synthesising processes comprising sonication and centrifugation, using no high-tech equipment. Three different preparation methods were systematically employed, using sonication and centrifugation techniques, to assess their competence in delivering homogenous deposition. The rGO suspensions were prepared using only deionised water (DIW), which is a low-cost technique that eliminates the use of chemicals and organic solvents. The yields of the rGO nanoflakes from the three methods, the deposition uniformity, the structural information and the morphological study are presented in this article. The most effective resulting preparation method was used to deposit the rGO nanoflakes onto Au-IDE devices to investigate their electrical performance. Two electrical measurement techniques such as electrochemical impedance spectroscopy (EIS) and I-V characterisation were used to characterise the as-prepared rGO/Au-IDE modified sensors.

2. Experimental Section

2.1 Materials and characterization techniques

The rGO powder was purchased from Graphitene Ltd, UK. Deionised water (DIW) was prepared using a laboratory water purification system (Sastec). Commercial gold interdigitated microelectrodes (Au-IDE) made on glass substrates were purchased from Metrohm Dropsens. The devices had dimensions of 7.6 mm x 22.8 mm (width x length). The Au-IDE had a gap

size of 5 μm, with a total of 500 fingers and an electrode length of 6760 μm. Titanium provided an adhesive layer between the gold and the glass substrates.

Ultraviolet-visible (UV-Vis) spectroscopy data was collected using a Lamdha 35 spectrophotometer (PerkinElmer, USA) to confirm the reduction of the purchased rGO powder. X-ray diffraction (XRD) was further used to assess this reduction and the associated structural information. The scan was recorded at Braggs angles of 5°- 80 ° in continuous fast mode, with a scanning rate of 0.02 degrees/second, using a Bruker D2 Phaser (Bruker Corporation, USA) operated at 30 kV and 10 mA with a Cu-Kα radiation wavelength of 1.54184 Å. Raman spectra were recorded using a Raman alpha300 R spectrometer (WITec GmbH, Germany) at a laser excitation wavelength of 532 nm. To visualise the deposition of rGO nanoflakes onto the glass substrates, optical images were collected using an Eclipse L300ND high powered microscope (HPM; Nikon Corporation, Japan) with a magnification of 5X, 10X, 20X and 50X. An SPA400 atomic force microscope (AFM; Seiko Instruments Inc., Japan) was used to analyse the surface morphologies and topographic heights of the rGO nanoflakes. The AFM measurements were performed using a tapping mode system. A Jeol JSM-6010LV scanning electron microscope (SEM; Jeol Ltd., Japan) was used to visualise the nanoflake morphologies and the SEM was operated at an operating voltage of 10 kV. Electrochemical impedance spectroscopy (EIS) measurements were performed using a Novocontrol alpha high-frequency analyser (Novocontrol Technologies GmbH, Germany). Meanwhile, current–voltage (I-V) measurements were performed using a PGSTAT204 potentiostat (Metrohm Autolab BV, Netherlands). All measurements were conducted at room temperature.

2.2 rGO preparation methods and optimisation

Two facile nanomaterial processing techniques such as sonication and centrifugation were systematically utilised to develop the three different preparation methods (see Figure 1). Briefly, in the first method, only ultrasonication was used and, in the second method, a combination of ultrasonication and centrifugation was used. In the third method, a post-sonication step was added to the second method. We named the preparation methods M1, M2 and M3 respectively, to simplify the discussion and elaboration in this paper. Detailed explanations of the rGO suspension preparation steps for M1, M2 and M3 are described below. Microscope glass slides were used to deposit the rGO suspensions. Prior to the deposition, the glass slides were cleaned with ethanol to remove undesirable organic or inorganic residues. The cleaning process was carried out by immersing the glass slides in ethanol container placed

in ultrasonic bath cleaner for 5 minutes and followed by rinsing 3 to 5 times with DIW. The remaining liquid was blow dried.

2.2.1 Method-1 (M1)

In a typical procedure, 10 mg of rGO powder was suspended in 10 mL of DIW with a concentration of 1 mg/mL, considered to be the initial concentration. This initial concentration was chosen based on concentrations that were used in recent studies [24,25]. The exfoliation process was then carried out by sonicating the suspension for 30 minutes in a 40 kHz ultrasonic bath cleaner. Thereafter, 10 µL of the as-prepared rGO suspension was immediately drop-cast onto a glass slide and followed by mild (50 ˚C) heat treatment to promote adhesion to the glass slide. After the droplet was completely dry, the glass slide was again rinsed 3-4 times with DIW to remove any unbound rGO, followed by drying in a convection oven at 50 ˚C until the glass slide was completely dry. The as-deposited rGO sample was then used for the characterisation.

2.2.2 Method-2 (M2)

A new rGO suspension with a concentration of 0.5 mg/mL was prepared in DIW and followed by ultrasonication for 1 hour. The rGO suspension was then centrifuged at 4000 rpm for 20 minutes. Next, the centrifuged suspension was carefully transferred to a vial, using a micropipette to avoid any intakes of large particles. Thereafter, 10 µL of the rGO suspension was immediately drop-cast onto a glass slide and followed by mild (50 ˚C) heat treatment. After the droplet dried completely, the glass slide was rinsed 3-4 times with DIW to remove any unbound rGO and followed by drying in a convection oven at 50 ˚C until the glass was completely dry. The as-deposited rGO sample was then used for the characterization.

2.2.3 Method-3 (M3)

The resulting rGO suspension that was prepared in M2 was further used in this method. Post-sonication was performed on the rGO suspension for 20 minutes, then 10 µL of the rGO suspension was immediately drop-cast onto a glass slide, and followed by mild (50 ˚C) heat treatment. After the droplet dried completely, the glass slide was rinsed 3-4 times with DIW to remove any unbound rGO nanoflakes and followed by drying in a convection oven at 50 ˚C

until the glass was completely dry. The as-deposited rGO sample was then used for the characterisation.

2.3 Electrochemical Impedance Spectroscopy and I-V measurements

Commercial Au-IDE with glass substrates were used to characterise the impedance and I-V characteristics. 35 µL of rGO suspension, prepared using M3, was drop-cast onto the Au-IDE devices and dried in a convection oven for 20 minutes at 50 °C to promote adhesion. The sensor was then rinsed 3-4 times with DIW to remove any unbound rGO nanoflakes. Thereafter, 50 µL of 10 mM PBS (pH 7.4), containing a mixture of 2 mM potassium hexacyanoferrate (III) and potassium hexacyanoferrate (II), $K_3[Fe(CN)_6]/K_4[Fe(CN)_6]$, was used as a redox probe and drop-cast onto the as-prepared rGO/Au-IDE modified sensors to characterise the impedance spectra. The EIS results were obtained by sweeping frequencies at a range of 0.1-100KHz at a 25 mV (V_{RMS}) amplitude of AC voltage. The Impedance spectra were observed for the real and imaginary parts of impedance, Z' and Z", respectively. Subsequently, I-V measurements were performed for a range of DC potentials from −2 to 2 V without any redox probes. All the measurements were carried out at room temperature.

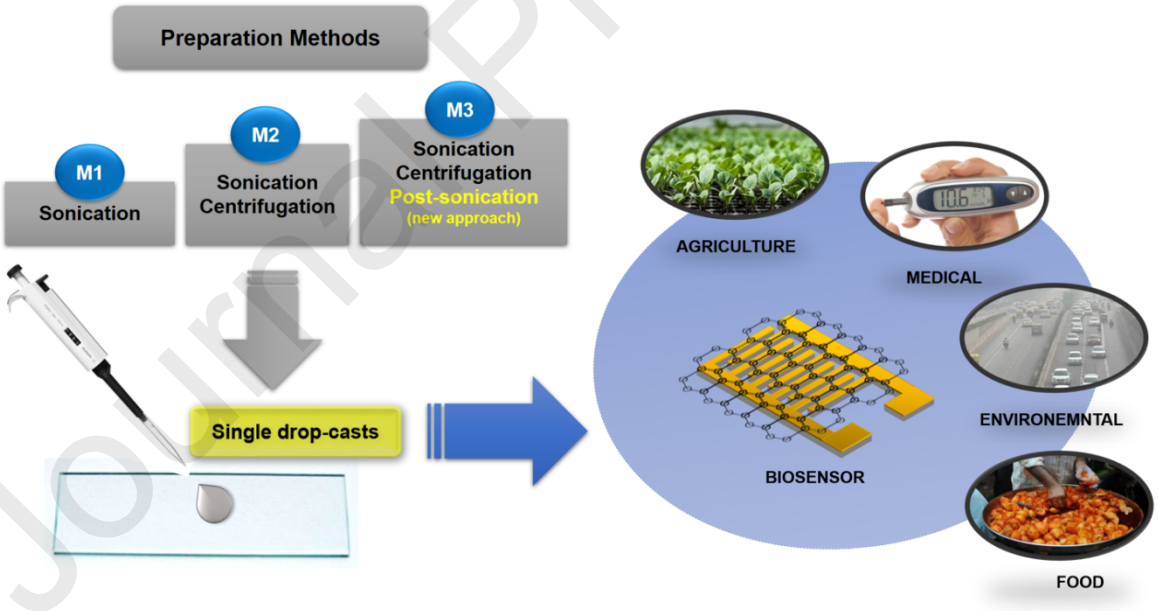

Figure 1: Illustration of three different preparation methods of rGO suspension. The three methods are denoted as M1, M2 and M3, respectively; shown with the related applications.

3. Results and Discussion

3.1 The yields of rGO nanoflakes in the DIW

The rGO suspensions were prepared using DIW and the yields of the rGO nanoflakes were assessed. The rGO displayed good dispersion behaviour in water, due to it containing functional oxygen groups and it also showed a stable dispersion, because of the electrostatic repulsion of negatively charged rGO sheets [26]. The use of DIW is considered to be a low-cost dispersion method compared to the use of chemical-based solvents, such as N-Methyl-2-Pyrrolidone (NMP). The deposition of rGO prepared in NMP requires a longer drying time especially when drying at a low temperature (50°C), because it has a high boiling point (202 °C). In addition, the use of DIW minimises any adulteration of the rGO nanoflakes.

Figure 2(a) shows the HPM results for the as-deposited rGO, deposited onto glass slide through single-droplet drop-casting for concentrations of 1 mg/mL, at magnifications of (i) 5X and (ii) 50X, respectively. The rGO nanoflakes were identified by a bright (white) flakes, which could be clearly seen at 50X magnification. The bright white flakes obviously indicated the production of multi-layers of rGO nanosheets, while a dull-flakes indicated the few layers. A previous study, suggested that such an observation results from the light reflection of an optical microscope when the thickness of rGO sheets varies [27]. Recently, a similar morphology was reported, but the deposition was carried out using multiple-droplet drop-casting [28]. The production of rGO nanoflakes for a concentration of 1 mg/mL showed a minimal number of white nanoflakes around the deposition region, which was largely covered by coarse black spots (see Figure 2 a(i)). The presence of coarse black spots indicated that the exfoliation process was incomplete; thus, a longer sonication duration (> 30 minutes) is recommended for exfoliating such a high (1 mg/mL) concentration of rGO in DIW.

In order to maximise the yields of rGO nanoflakes and minimise the coarse black spots, three new sets of rGO suspensions were prepared by reducing the concentration levels gradually. The three new sets of rGO suspensions had concentrations of 0.5-, 0.2-, 0.1-mg/mL, which were 2, 5, and 10 times lower than the initial concentration of 1 mg/mL, respectively. The sonication duration for the three sets was increased to 1 hour compared to the initial sonication duration of 30 minutes for improved evaluation. Figures 2(b), 2(c) and 2(d) shows the as-deposited rGO for concentrations of 0.5- 0.2- and 0.1-mg/mL, respectively, at magnifications of (i) 5X and (ii) 50X. As expected, the presence of coarse black spots was significantly reduced for the three concentrations when compared to the initial concentration of 1 mg/mL. Moreover, large numbers of rGO (white) nanoflakes were observed for a

concentration of 0.5 mg/mL (see Figures 2b(i) and 2b(ii)), but only a few nanoflakes were observed for concentrations of 0.2- and 0.1-mg/mL (see Figures 2c(ii) and 2d(ii), respectively). Clearly, the incremental increase in the sonication duration contributed to improved exfoliation, resulting in larger yields for a concentration of 0.5 mg/mL. However, only very small numbers of nanoflakes were observed for concentrations of 0.2- and 0.1-mg/mL due to concentrations being very low. The micropipette aspirating only very small numbers of nanoflakes explained the lower coverage in the deposition region for both concentrations (0.2- and 0.1-mg/mL) deposited through the single-droplet drop-casting technique. In summary, a concentration of 0.5 mg/mL and the sonication duration of 1 hour were considered to be the optimum parameters for producing large numbers of rGO nanoflakes in DIW.

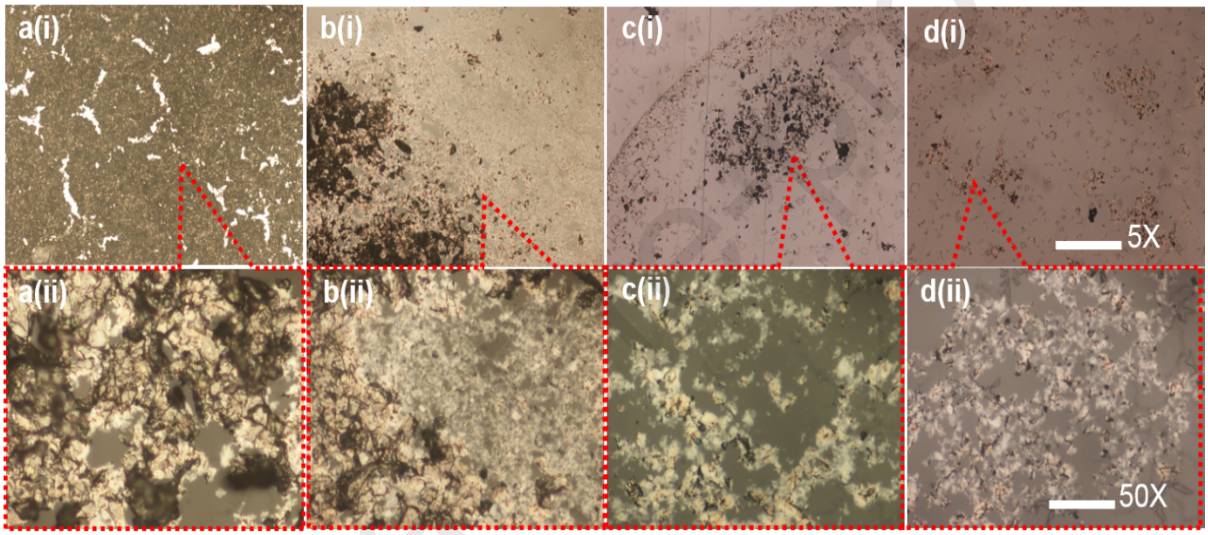

Figure 2: HPM images of (white) rGO nanoflakes deposited through single-droplet drop-casting onto glass slides for the various concentrations. Images (a), (b), (c) and (d) show rGO with concentrations of 1-, 0.5-, 0.2- and 0.1-mg/mL, respectively, at magnifications of (i) 5X and (ii) 50X. The sonication duration for (a) was 30 minutes and, for (b), (c) and (d) was 1 hour.

3.2 Assessment on the developed methods and repeatability test

A large yield of rGO nanoflakes was observed for a concentration of 0.5 mg/mL; thus, this concentration was further used to study the deposition uniformity. Three different preparation methods were systematically employed to prepare the rGO suspensions, representing the methods M1, M2 and M3, respectively. The as-prepared rGO suspensions from each method were immediately deposited onto glass substrates through a single-droplet drop-casting approach. Briefly, in M1, only ultrasonication was used to prepare the rGO

suspension. In M2, ultrasonication followed by centrifugation to prepare the suspension and in M3, a post-sonication was applied to the suspension resulting from M2. In fact, each method was employed in an effort to obtain a large uniform network of self-assembled rGO nanoflakes through the single-droplet drop-casting technique.

Figures 3 (A), (B) and (C) present the digital images of the rGO suspensions prepared using M1, M2 and M3, respectively. Figures 3 (a), (c) and (e) show the digital images of the as-deposited rGO, prepared using M1, M2 and M, respectively, deposited through single-droplet drop-casting technique. The rGO suspension prepared using M1 showed darker dispersion than the suspensions from M2 and M3, because larger and coarser particles existed in the M1 suspension which explains the rGO was not completely exfoliated. The digital image in Figure 3 (a), clearly shows the darker deposition from the M1 suspension compared to the deposition from the M2 and M3 suspensions, (Figures 3 (c) and (e)), respectively. The depositions from the M2 and M3 suspensions were very smooth, thin and light-coloured, because the centrifugation significantly isolated the coarse particles. Figures 3 (b), (d) and (f) show the HPM results for the depositions from the M1, M2 and M3 suspensions, respectively, and (i), (ii) and (iii) show magnifications of 10X, 20X and 50X, respectively. Large numbers of rGO nanoflakes, together with black spots and some empty spaces (highlighted in blue) were clearly seen for the M1 deposition (see Figure 3 (b)). The coarse particles were clearly observed and identified as black spots, explaining the darker deposition. Moreover, the self-assembled rGO nanoflakes were seen to form a larger clustered network. This network was very tight and network was firmly attached to the glass surface, because the network was not removed, even when rinsed 3-4 times with DIW. The deposition from M1 alone produced a very coarse distribution with a mixture of nanoflakes and black spots. The black spots were completely removed in M2 and M3 because of the centrifugation (see Figures 3 (d), 3 (f)). The drop-casting in M2 and M3 produced rGO nanoflakes that exhibited a very smooth, thin appearance and homogenously covered a certain region within the droplet area. Nevertheless, the deposition from M2 (see Figure 3 (d)) exhibited a lot of empty spaces compared to the deposition from M3 (see Figure 3 (f)). Therefore, the post-sonication step in M3 enabled homogenous deposition through the single-droplet drop-casting technique. Furthermore, the deposition from M3 was very uniform and large self-assembled rGO nanoflake networks were observed with very few empty spaces.

The deposition repeatability and homogeneity of the single-droplet drop-casting were tested for M2 and M3 with an extra two droplets drop-cast onto the glass substrates (see Figures

3 (c) and 3 (e)). We found a similar pattern of deposition coverage, and which remained consistent for every drop-cast.

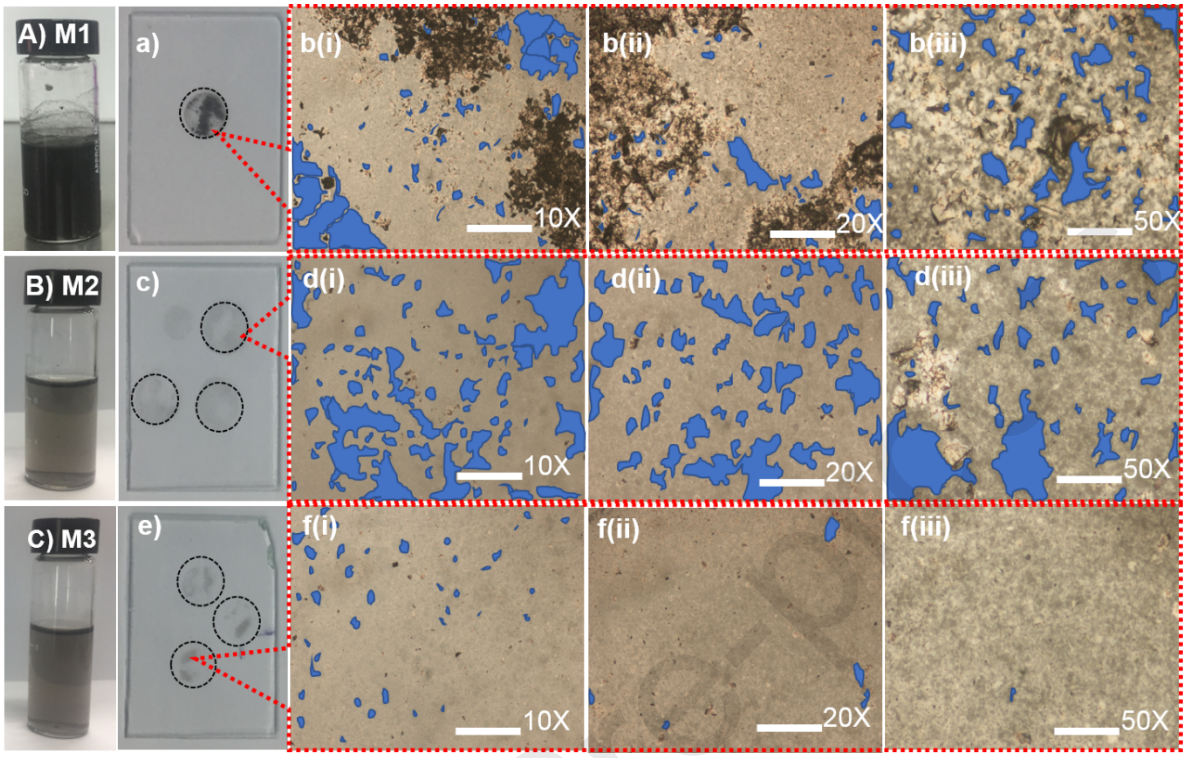

Figure 3: Digital and HPM images. (A), (B) and (C) show digital images of the rGO suspensions prepared using M1, M2 and M3, respectively. Meanwhile (a), (c) and (e) show digital images of the as-deposited rGO prepared using M1, M2 and M3, respectively and deposited through single-droplet drop-casting onto glass slides. Images (b), (d) and (f) show the HPM results for the depositions from M1, M2 and M3, respectively and (i), (ii), and (iii) show the depositions at magnifications of 10X, 20X and 50X, respectively.

3.3 Surface morphology analyses of the white-nanoflakes

The morphology of the as-deposited rGO nanoflakes resulting from M3 was further analysed using atomic force microscope imaging. Figures 4 (a) and (b) show the topographic heights of the rGO nanoflakes and their 3D images under the AFM. The images clearly revealed that the nanoflakes exhibited a random thickness, ranging from ~1.1 nm to nearly 100 nm with densely clustered networks (see Figures S1 and S2). However, most of the rGO nanoflakes were below 10 nm, with a lateral dimension of more than 1 µm. The AFM images confirmed the HPM results, with the dull nanoflakes being very thin compared to the bright nanoflakes, confirming the production of few and multiple layers of rGO nanoflakes, respectively (see

Figure 4 (a)). Moreover, the morphology of the rGO nanoflakes was wrinkled, invariably crumpled and having a wave-like structure, as well as forming a large network. Such an imbalanced morphology was due to the unevenness of graphite oxidation and the exfoliation process [27]. Furthermore, the SEM image clearly displayed such attributes and further revealed that the deposition largely and homogenously engulfed the droplet region as seen in Figure 4 (c) (see Figure S3 at different magnifications). It is worth mentioning that the choice of SEM operating voltage played an important role in capturing a good quality image, because the type of substrates used determined the clarity of the image captured. Hence, a low operating voltage is recommended for non-conductive substrates when working with rGO nanoflakes.

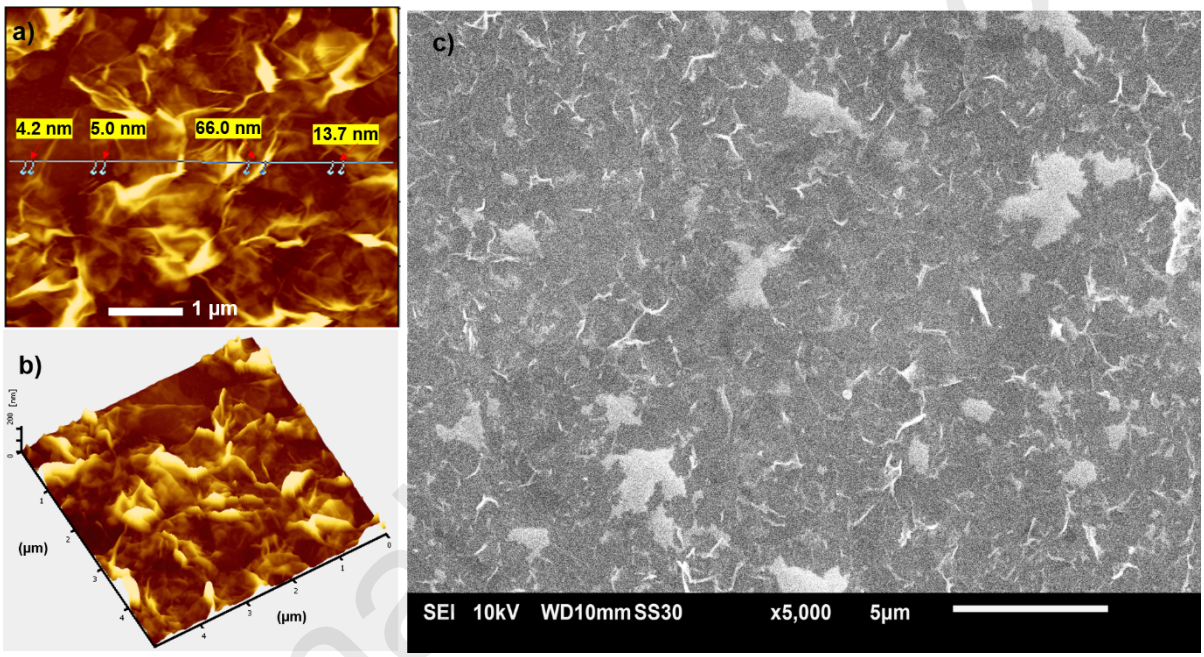

Figure 4: AFM images of rGO nanoflakes, with (a) and (b) showing the topographic heights of the nanoflakes and their 3D images, respectively; (c) shows a SEM image of the rGO nanoflakes.

3.4 Validation on the rGO and structural analysis

3.4.1 *UV-Vis Spectroscopy*.

UV-Vis spectroscopy was used to characterise the reduction peaks of the rGO. The maximum absorption peak of the rGO in the DIW was observed at 273 nm, with a broad shoulder (Figure 5 (a)). This observation was similar to the GO reduction reported by Luo et al. [29], where the maximum absorption peak shifted to a higher wavelength (> 270 nm) when the reduction process was carried out using a high temperature. In previous studies, the maximum absorption

peak of GO was observed at ranges of 225 nm [14], 228 nm [30] and 230 nm [31] and the maximum absorption peak of the rGO was normally reported to shift to higher wavelengths such as 269 nm [32] or 270 nm [33] suggesting that reduction occurred. Such a shifting phenomenon in UV-Vis absorption is due to the removal of some oxygen-containing groups and the restoration of pi-conjugated networks. The UV-Vis absorption spectra therefore confirmed that the material had undergone a reduction process.

3.4.2 *X-ray Diffraction (XRD) Analysis.*

XRD was used to further confirm the de-oxygenation and to gather structural information about the rGO. In this work, the 2 theta angle for the rGO was observed, at 23.3˚ to have a weaker and broader diffraction pattern (see Figure 5 (b)), which was in line with previous studies, thus confirming the reduction process [34,35]. The weaker and broader diffraction pattern described the deterioration in the rGO crystalline structure [36]. Generally, a sharp diffraction peak for pristine graphite is observed at angles of 26˚ to 26.5˚ [30,34] and such 2 theta angles reveal that the pristine graphite exhibits a highly organized hexagonal structure with an interlayer distance (d-spacing) of 3.36 Å. However, when the diffraction angle is < 26˚, it is easy to notice that the material had gone through an oxidation process. Furthermore, highly oxidized GO has diffraction peaks at very low angles, usually in the range of 9˚-10˚ [37,38,27]. Clearly, this comparative study showed that the reduction process can be determined by observing x-ray diffraction peak angles between 9˚ and 26˚. A high diffraction angle, such as 23.3˚ or close to 26˚ indicates that large numbers of oxygen-containing groups have been removed while a sharp peak show that the material retains its highly crystalline structure.

3.4.3 *Raman Characterisation.*

Raman characterisation spectroscopy was performed to analyse the structural and electronic features of the rGO nanoflakes. Two distinctive spectra of graphene were represented by the D- and G-peaks at wavenumbers of 1350 cm^{-1} and 1590 cm^{-1}, respectively [39]. Figure 5 (c) displays the Raman spectra for the rGO with the D-peak at 1357 cm^{-1} and the G-peak at 1590 cm^{-1}, further validating the material as rGO. Notably, the D-band indicated the defects in the hexagonal carbon lattice while the G-band was due to a doubly degenerate zone center in the E_{2g} mode. The quality of the rGO nanoflakes was estimated by calculating the intensity ratio of the D- and G- peaks which indicated the degree of disorder of the nanoflakes. The peak intensity of the G-band was found to be slightly higher than the peak of the D-band, which

indicated the effectiveness of the restoration of hexagonal networks of carbon sp^2 atoms with an intensity ratio (I_D/I_G) of 0.96 suggesting a lower degree of defectiveness [8].

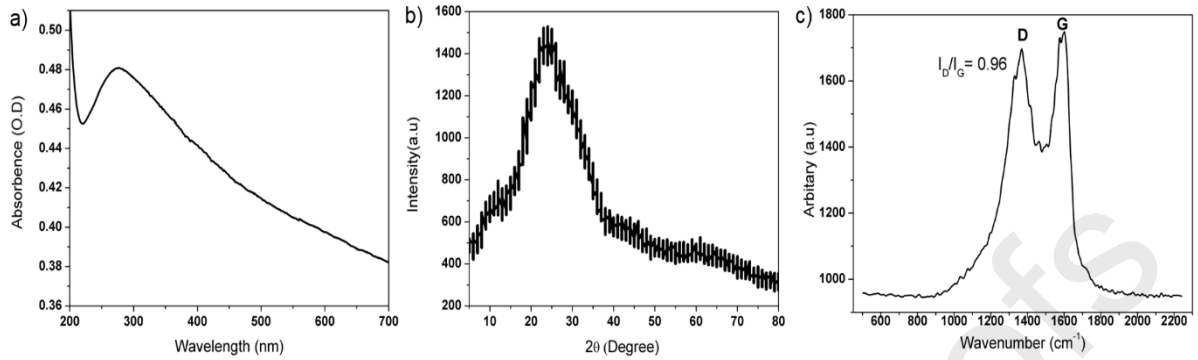

Figure 5: (a) shows the UV-Vis absorption spectra of rGO,. scanned at wavelengths from 200 to 700 nm, with the maximum absorption peak at 273 nm;, (b) shows the XRD pattern of rGO, with the 2 theta peak angle appearing at ~23 degrees and (c) shows the Raman spectra of the rGO measured at spectral wavenumbers ranging from 500-2250 cm^{-1}.

3.5 Impedance spectra and reproducibility assessments

The electrical performance of the self-assembled rGO nanoflake networks was characterised using commercial Au-IDE. Figures 6A and 6B show the Au-IDE before and after the deposition with rGO nanoflakes, respectively. The as-deposited rGO nanoflakes were prepared using M3. The deposition region on the Au-IDE' surfaces was slightly darker than on the bare devices, illustrating the distribution of the rGO nanoflakes. To validate the distribution and deposition of the rGO nanoflakes, the device was further characterised using an HPM and a 3D profilometer. Figures 6 a(i) and b(i) show the HPM images before and after the deposition of the rGO nanoflakes, respectively. Meanwhile Figures 6 a(ii) and 6 b(ii) show the 3D images before and after deposition with the rGO nanoflakes, respectively. The rGO nanoflakes were observed to be very evenly distributed within the device and firmly attached to the device's surface. This was because the nanoflakes were not removed, even after being rinsed 3-4 times with DIW.

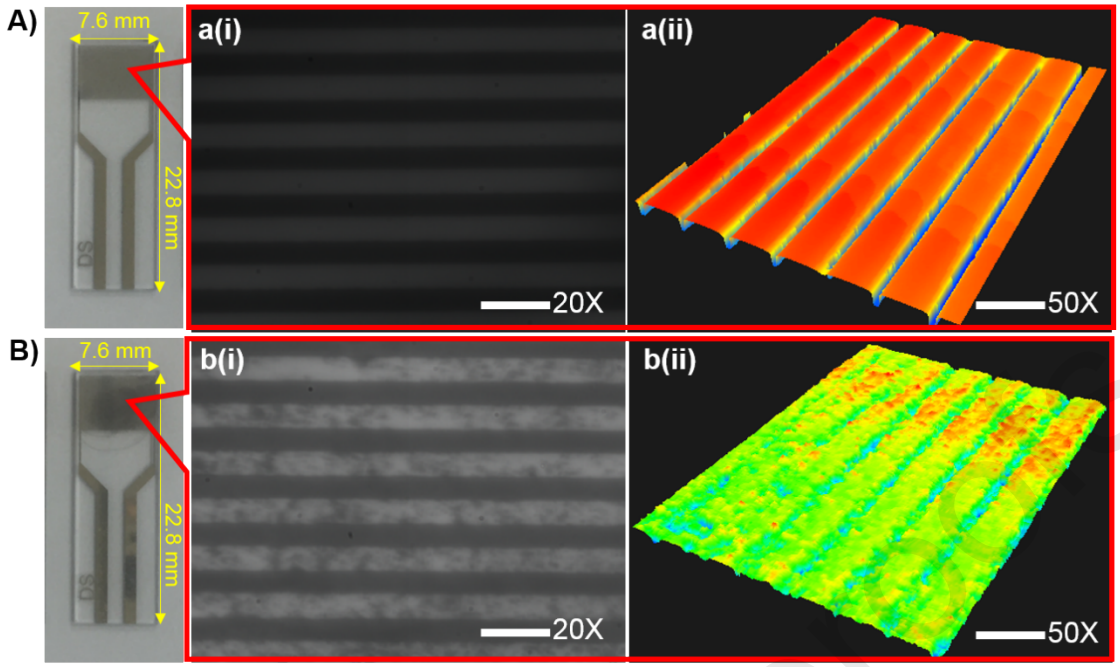

Figure 6: Digital images (A) and (B) show the Au-IDE before and after the modification with rGO nanoflakes, respectively. The HPM images a(i) and b(i) show the bare electrode surface and the deposition of rGO nanoflakes, respectively. The 3D images a(ii) and b(ii) show the bare electrode surface and the modification with rGO nanoflakes, respectively.

Three devices were utilised to perform the EIS test, with measurements carried out with and without modification by rGO nanoflakes. The Nyquist plots for the three devices, before and after the modification with rGO nanoflakes are shown in Figures 7(a) and 7(b), respectively. The semicircle profile explained that the characteristics of the double layer capacitance (C_{dl}) were in parallel with the electron charge transfer resistance (R_{ct}) components [40]. A Randles equivalent circuit (see Figure 7 a(i) inset) can be used to express Nyquist plots, with R_s, R_{ct} and C_{dl} representing the redox probe solution resistances of the 2mM $K_3[Fe(CN)_6]/K_4[Fe(CN)_6]$, the charge transfer resistance and the double layer capacitance, respectively. The average values of the redox probe solution resistances (R_s) (see Figure 7 a(ii) inset) and the charge transfer resistance (R_{ct}) for the bare devices were 53 Ω and 226 kΩ, respectively. The average values were calculated because the volume of the redox probe' solution drop-casting may have affected the dissolved ion concentration on the devices' surfaces. Furthermore, the slight variation in the semicircle diameter for the real part impedance (Z') indicated that the bare devices may not have been completely free of contaminants.

The rGO/Au-IDE modified sensors (see Figure 7 b(i) inset) showed a tremendous reduction in the impedance spectra (real part, Z' and imaginary part, Z"), as can been seen in

Figure 7 (b), when compared to the bare devices (Figure 7 (a)). This suggested that the rGO nanoflakes modified with Au-IDE exhibited excellent electron mobility, with the modification enhancing the electrical conductivity approximately ~1000 fold compared to the bare devices. This was because the homogenous deposition of very thin rGO nanoflakes (prepared using M3) facilitated electron mobility. Such an enhancement is favourable for developing chemical sensors or biosensors, because a large number of bio-receptors can be immobilised on the rGO nanoflakes' surfaces leading to ultrasensitive detection.

The sensor reproducibility tests were conducted using three bare Au-IDE devices and the rGO nanoflakes deposited from M3 with the same single-droplet drop-casting procedure. It was noted that the impedances of the real parts (Z') for the rGO/Au-IDE modified sensors (at the lowest frequency) were within a range of hundred ohms (~230-330 Ω) with an almost similar trend (see Figure 7 (b)). However, the small variation in the real parts (Z') was due to the possibility that the number of rGO nanoflakes deposited varied slightly from device to device, caused by the random dispersion of the rGO nanoflakes in DIW.

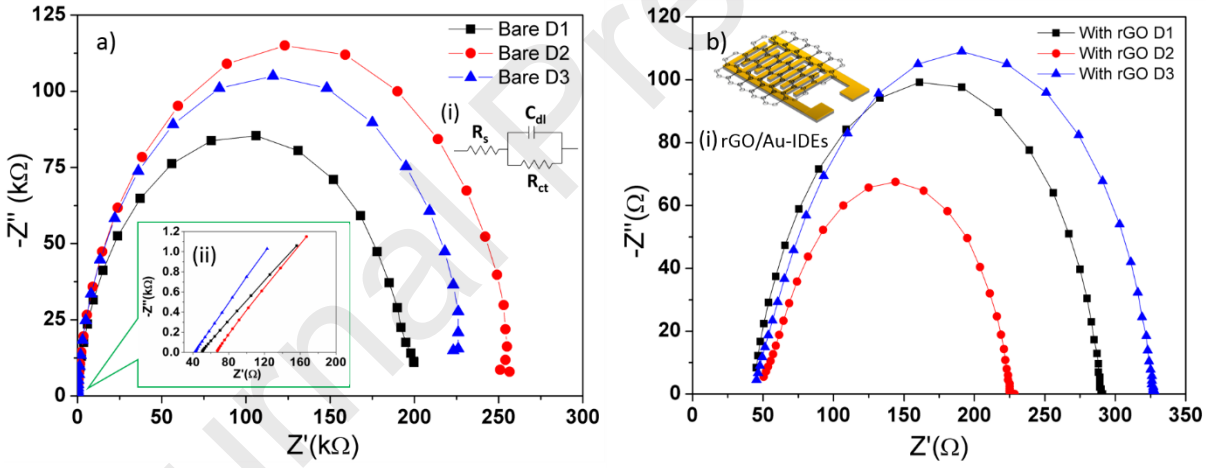

Figure 7**:** Electrochemical impedance spectroscopy. The Nyquist plots for the three devices: (a) bare devices and (b) after modification with rGO nanoflakes, respectively. Inset (a) shows the Randles equivalent circuit and inset (b) shows the rGO/Au-IDE modified sensors.

3.6 I-V curve characteristics

The I-V curves were further assessed to validate the electrical conductivity of the rGO/Au-IDE modified sensors. The I-V curves for the three sensors are shown in Figure 8 and were biased with DC potentials ranging from -2 to 2 V and the inset shows the I-V profile for the bare device. It was observed that the bare device had an average current conductivity of 8.1

μA. This result suggested that the Au-IDE acted as open circuits when biasing DC potentials which is a well-known characteristic of capacitor-based electrodes. However, linear ohmic current conductivity was observed for the rGO/Au-IDE modified sensors with bipolar electronic transport characteristics. The current conductivities of the rGO modified sensors were enhanced up to ~1000 fold (reaching mA) compared to the bare devices. The I-V profiles further revealed that the sensors had no short circuit characteristics confirming that the sensors operated as resistors in the DC biasing condition.

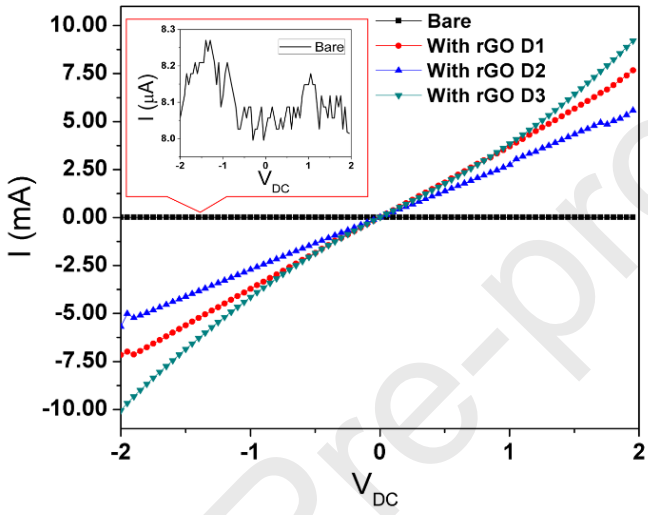

Figure 8: I-V curves for the rGO/Au-IDE modified sensors.

4. Conclusion

In this article, a facile approach to obtaining a homogenous self-assembly of rGO nanoflake networks through single-droplet drop-casting was demonstrated. The rGO suspensions were prepared using only deionised water, which is considered to be a low-cost preparation method. A large self-assembly of rGO nanoflake networks was achieved by employing only existing nanomaterial processing technology (sonication and centrifugation), with no high-tech equipment. Three different preparation methods were systematically employed to prepare the final rGO colloidal suspensions. We found that M3 displayed very good deposition of rGO nanoflakes onto glass substrates, which formed large self-assembled and clustered networks resulting from post-sonication. Furthermore, M3 also displayed the ability to produce a very thin layer (~1.1 nm) of rGO nanoflakes with highly interconnected networks. A concentration of 0.5 mg/mL and a sonication duration of one hour were considered to be the optimum parameters for producing large numbers of rGO nanoflakes in DIW.

Moreover, the impedance spectra and the I-V characteristics further revealed that the rGO nanoflakes, modified with Au-IDE sensors, exhibited excellent electron mobility when the charge transfer resistance declined approximately ~1000 fold compared to the bare device. This research has provided new insights for homogenously depositing large networks of rGO nanoflakes, using an inexpensive laboratory tool (a micropipette) and single-droplet drop-casting. Furthermore, the post-sonication technique can be applied to synthesis other 2D nanomaterials in an effort to develop low-cost bio/chemical sensors.

Acknowledgement

The author would like to acknowledge the support of the Fundamental Research Grant Scheme (FRGS), under grant number FRGS/1/2017/STG05/UNIMAP/03/3 from the Ministry of Education Malaysia.

References

[1] H. Bi, S. Wan, X. Cao, X. Wu, Y. Zhou, K. Yin, S. Su, Q. Ma, M. Sindoro, J. Zhu, Z. Zhang, H. Zhang, L. Sun, A general and facile method for preparation of large-scale reduced graphene oxide films with controlled structures, Carbon N. Y. 143 (2019) 162–171. doi:10.1016/j.carbon.2018.11.007.

[2] U.A. Méndez-Romero, S.A. Pérez-García, X. Xu, E. Wang, L. Licea-Jiménez, Functionalized reduced graphene oxide with tunable band gap and good solubility in organic solvents, Carbon N. Y. 146 (2019) 491–502. doi:10.1016/j.carbon.2019.02.023.

[3] C. Ingrosso, M. Corricelli, A. Disha, E. Fanizza, G. V. Bianco, N. Depalo, A. Panniello, A. Agostiano, M. Striccoli, M.L. Curri, Solvent dispersible nanocomposite based on Reduced Graphene Oxide in situ decorated with gold nanoparticles, Carbon N. Y. 152 (2019) 777–787. doi:10.1016/j.carbon.2019.06.070.

[4] S. Kumar, S.D. Bukkitgar, S. Singh, Electrochemical Sensors and Biosensors Based on Graphene Functionalized with Metal Oxide Nanostructures for Healthcare Applications, Chem. Sel. 4 (2019) 5322–5337. doi:10.1002/slct.201803871.

[5] N.P. Shetti, D.S. Nayak, S.J. Malode, R.M. Kulkarni, D.B. Kulkarni, R.A. Teggi, V. V Joshi, Electrooxidation and determination of flufenamic acid at graphene oxide modified carbon electrode, Surfaces and Interfaces. 9 (2017) 107–113. doi:10.1016/j.surfin.2017.08.008.

[6] X. Zhang, X. Wang, F. Meng, J. Chen, S. Du, Broadband and strong electromagnetic wave absorption of epoxy composites filled with ultralow content of non-covalently

modified reduced graphene oxides, Carbon N. Y. 154 (2019) 115–124. doi:10.1016/j.carbon.2019.07.076.

[7] T. Xu, D. Yang, Z. Fan, X. Li, Y. Liu, C. Guo, M. Zhang, Z.Z. Yu, Reduced graphene oxide/carbon nanotube hybrid fibers with narrowly distributed mesopores for flexible supercapacitors with high volumetric capacitances and satisfactory durability, Carbon N. Y. 152 (2019) 134–143. doi:10.1016/j.carbon.2019.06.005.

[8] R. Shu, G. Zhang, J. Zhang, X. Wang, M. Wang, Y. Gan, J. Shi, J. He, Fabrication of reduced graphene oxide/multi-walled carbon nanotubes/zinc ferrite hybrid composites as high-performance microwave absorbers, J. Alloys Compd. 736 (2018) 1–11. doi:10.1016/j.jallcom.2017.11.084.

[9] N.P. Shetti, S.J. Malode, D.S. Nayak, G.B. Bagihalli, K.R. Reddy, K. Ravindranadh, C.V. Reddy, A novel biosensor based on graphene oxide-nanoclay hybrid electrode for the detection of Theophylline for healthcare applications, Microchem. J. 149 (2019) 103985. doi:10.1016/j.microc.2019.103985.

[10] M.Z.B. Dzukarnain, T. Takami, H. Imai, T. Ogino, Highly conductive, monolayer and large-area reduced graphene oxide films fabricated by electrical connection at the two-dimensional boundaries between the tiled graphene oxide flakes, Thin Solid Films. 615 (2016) 247–255. doi:10.1016/j.tsf.2016.07.029.

[11] M. Soni, P. Kumar, J. Pandey, S.K. Sharma, A. Soni, Scalable and site specific functionalization of reduced graphene oxide for circuit elements and flexible electronics, Carbon N. Y. 128 (2018) 172–178. doi:10.1016/j.carbon.2017.11.087.

[12] S.R. Kasjoo, M.M. Ramli, M.R. Zakaria, M.K.M. Arshad, A Field-Effect Device Based on an Exfoliated Thin Film of Few-Layer Graphene, IEEE-ICSE2014 Proc. 2014, Kuala Lumpur, Malaysia. (2014) 370–372. doi:10.1109/SMELEC.2014.6920874.

[13] X.-N. Xu, X.-N. Guan, H.-H. Zhou, Y.-F. Zhu, One-Step Reduction and Surface Modification of Graphene Oxide by 3-Hydroxy-2-Naphthoic Acid Hydrazide and Its Polypropylene Nanocomposites, Nanomaterials. 7 (2017) 25. doi:10.3390/nano7020025.

[14] P. Chettri, V.S. Vendamani, A. Tripathi, M.K. Singh, A.P. Pathak, A. Tiwari, Green synthesis of silver nanoparticle-reduced graphene oxide using Psidium guajava and its application in SERS for the detection of methylene blue, Appl. Surf. Sci. 406 (2017) 312–318. doi:10.1016/j.apsusc.2017.02.073.

[15] U. Hashim, R. Adzhri, M.K.M. Arshad, M.F.M. Fathil, A.R. Ruslinda, R.M. Ayub, M.N.M. Nuzaihan, A.H. Azman, M. Zaki, A.B. Suriani, Spray pyrolysis of graphene oxide for field-effect transistor biosensor application, Proc. - 2015 2nd Int. Conf. Biomed. Eng. ICoBE 2015. (2015) 30–31. doi:10.1109/ICoBE.2015.7235909.

[16] E. Rokhsat, O. Akhavan, Improving the photocatalytic activity of graphene oxide/ZnO nanorod films by UV irradiation, Appl. Surf. Sci. 371 (2016) 592–595. doi:10.1016/j.apsusc.2016.02.222.

[17] B. Cai, S. Wang, L. Huang, Y. Ning, Z. Zhang, G.J. Zhang, Ultrasensitive label-free detection of PNA-DNA hybridization by reduced graphene oxide field-effect transistor

biosensor, ACS Nano. 8 (2014) 2632–2638. doi:10.1021/nn4063424.

[18] R. Kumar, R.M. Kumar, P. Bera, S. Ariharan, D. Lahiri, I. Lahiri, Temperature-time dependent transmittance, sheet resistance and bonding energy of reduced graphene oxide on soda lime glass, Appl. Surf. Sci. 425 (2017) 558–563. doi:10.1016/j.apsusc.2017.06.224.

[19] Y. Liu, D. Zhang, Y. Shang, C. Guo, A simple and efficient electrochemical reductive method for graphene oxide, Bull. Mater. Sci. 37 (2014) 1529–1533. doi:10.1007/s12034-014-0107-1.

[20] W. Dong, Y. Ren, Y. Zhang, Y. Chen, C. Zhang, Z. Bai, R. Ma, Q. Chen, Synthesis of Pb nanowires-Au nanoparticles nanostructure decorated with reduced graphene oxide for electrochemical sensing, Talanta. 165 (2017) 604–611. doi:10.1016/j.talanta.2017.01.017.

[21] B. Li, A. Yu, G. Lai, Self-assembly of phenoxyl-dextran on electrochemically reduced graphene oxide for nonenzymatic biosensing of glucose, Carbon N. Y. 127 (2018) 202–208. doi:10.1016/j.carbon.2017.10.096.

[22] O.J.D. Souza, R.J. Mascarenhas, A.K. Satpati, M.B. Basavanakote, A novel ZnO / reduced graphene oxide and Prussian blue modified carbon paste electrode for the sensitive determination of Rutin, Sci. China Chem. 62 (2019) 262–270.

[23] G. Manasa, R.J. Mascarenhas, A.K. Satpati, B.M. Basavaraja, S. Kumar, An electrochemical Bisphenol F sensor based on ZnO/G nano composite and CTAB surface modified carbon paste electrode architecture, Colloids Surfaces B Biointerfaces. 170 (2018) 144–151. doi:10.1016/j.colsurfb.2018.06.002.

[24] A.C. Faucett, J.N. Flournoy, J.S. Mehta, J.M. Mativetsky, Evolution, structure, and electrical performance of voltage-reduced graphene oxide, FlatChem. 1 (2017) 42–51. doi:10.1016/j.flatc.2016.10.003.

[25] Y. Wang, H. Sauriat-Dorizon, H. Korri-Youssoufi, Direct electrochemical DNA biosensor based on reduced graphene oxide and metalloporphyrin nanocomposite, Sensors Actuators B Chem. 251 (2017) 40–48. doi:10.1016/j.snb.2017.04.128.

[26] D. Konios, M.M. Stylianakis, E. Stratakis, E. Kymakis, Dispersion behaviour of graphene oxide and reduced graphene oxide, J. Colloid Interface Sci. 430 (2014) 108–112. doi:10.1016/j.jcis.2014.05.033.

[27] H. Saleem, M. Haneef, H.Y. Abbasi, Synthesis route of reduced graphene oxide via thermal reduction of chemically exfoliated graphene oxide, Mater. Chem. Phys. 204 (2018) 1–7. doi:10.1016/j.matchemphys.2017.10.020.

[28] C. Van Nguyen, R. Bartali, L. Crema, G. Speranza, Effect of glass surface treatments on the deposition of highly transparent reduced graphene oxide films by dropcasting method, Colloids Surfaces A Physicochem. Eng. Asp. 498 (2016) 231–238. doi:10.1016/j.colsurfa.2016.03.051.

[29] D. Luo, G. Zhang, J. Liu, X. Sun, Evaluation criteria for reduced graphene oxide, J. Phys. Chem. C. 115 (2011) 11327–11335. doi:10.1021/jp110001y.

[30] J. Wang, E. Caliskan, Š. Lidija, Green reduction of graphene oxide using alanine,

Mater. Sci. Eng. C. 72 (2017) 1–6. doi:10.1016/j.msec.2016.11.017.

[31] S.C.B. Gopinath, P. Anbu, T. Theivasanthi, T. Lakshmipriya, C. Hong, V. Kannaiyan, P. Palaniyandi, V. Suresh, Characterization of reduced graphene oxide obtained from vacuum- assisted low-temperature exfoliated graphite, Microsyst. Technol. 3 (2018) 5007–5016. doi:10.1007/s00542-018-3921-3.

[32] C. Chen, J. Li, R. Li, G. Xiao, D. Yan, Synthesis of superior dispersions of reduced graphene oxide, New J. Chem. 37 (2013) 2778. doi:10.1039/c3nj00304c.

[33] M. Nasrollahzadeh, S. Mohammad Sajadi, A. Rostami-Vartooni, M. Alizadeh, M. Bagherzadeh, Green synthesis of the Pd nanoparticles supported on reduced graphene oxide using barberry fruit extract and its application as a recyclable and heterogeneous catalyst for the reduction of nitroarenes, J. Colloid Interface Sci. 466 (2016) 360–368. doi:10.1016/j.jcis.2015.12.036.

[34] A.H. Lima, J.P. Mendonça, M. Duarte, F. Stavale, C. Legnani, G.S.G. De Carvalho, Reduced graphene oxide prepared at low temperature thermal treatment as transparent conductors for organic electronic applications, Org. Electron. 49 (2017) 165–173. doi:10.1016/j.orgel.2017.05.054.

[35] T. Wang, H. Guo, X. Chen, M. Lu, Low-temperature thermal reduction of suspended graphene oxide fi lm for electrical sensing of DNA-hybridization, Mater. Sci. Eng. C. 72 (2017) 62–68. doi:10.1016/j.msec.2016.11.026.

[36] K.K.H. De Silva, H.H. Huang, M. Yoshimura, Progress of reduction of graphene oxide by ascorbic acid, Appl. Surf. Sci. 447 (2018) 338–346. doi:10.1016/j.apsusc.2018.03.243.

[37] H. Feng, R. Cheng, X. Zhao, X. Duan, J. Li, A low-temperature method to produce highly reduced graphene oxide, Nat. Commun. 4 (2013) 1537–1539. doi:10.1038/ncomms2555.

[38] T. Thomas, R.J. Mascarenhas, C. Nethravathi, M. Rajamathi, B.E.K. Swamy, Graphite oxide bulk modified carbon paste electrode for the selective detection of dopamine : A voltammetric study, J. Electroanal. Chem. 659 (2011) 113–119. doi:10.1016/j.jelechem.2011.05.011.

[39] S. Grimm, M. Schweiger, S. Eigler, J. Zaumseil, High-Quality Reduced Graphene Oxide by CVD-Assisted Annealing, J. Phys. Chem. C. 120 (2016) 3036–3041. doi:10.1021/acs.jpcc.5b11598.

[40] S. Azzouzi, W.C. Mak, K. Kor, A.P.F. Turner, M. Ben Ali, V. Beni, An integrated dual functional recognition/amplification bio-label for the one-step impedimetric detection of Micro-RNA-21, Biosens. Bioelectron. 92 (2017) 154–161. doi:10.1016/j.bios.2017.02.014.

CRediT authorship contribution statement

S. Taniselass: Conceptualization, Methodology, Investigation, Data curation, Formal analysis, Writing - original draft, Writing - review & editing. **M.K. Md Arshad:**

Conceptualization, Data curation, Methodology, Funding acquisition, Project administration, Supervision, Validation, Writing - review & editing.
Subash C.B. Gopinath: Data curation, Supervision, Validation, Writing- review & editing.
Muhammad M Ramli: Data curation, Validation, Writing- review & editing.

Declaration of Interest/Ethical Statement

I testify on behalf of all co-authors that our article submitted to Journal of Colloid and Interface Science:

Title: Self-Assembled Reduced Graphene Oxide Nanoflakes Assisted by Post-Sonication Boosted Electrical Performance in Gold Interdigitated Microelectrodes

All authors: S. Taniselass, M.K. Md Arshad, Subash C.B. Gopinath , Muhammad M Ramli

That;

1) this material has not been published in whole or in part elsewhere;
2) the manuscript is not currently being considered for publication in another journal;
3) all authors have been personally and actively involved in substantive work leading to the manuscript, and will hold themselves jointly and individually responsible for its content.

Date: 30th December 2019

Corresponding author:

Assoc. Prof. Ir. Dr. Mohd Khairuddin Md Arshad
Tel: +604-9798581; Fax: +604-9798578
Email: mohd.khairuddin@unimap.edu.my

627

628

629

630

631